Brr6 plays a role in gene recruitment and transcriptional regulation at the nuclear envelope

Anne de Bruyn Kops*, Jordan E. Burke, and Christine Guthrie*
Department of Biochemistry and Biophysics, University of California, San Francisco, San Francisco, CA 94143

ABSTRACT **Correlation between transcriptional regulation and positioning of genes at the nuclear envelope is well established in eukaryotes, but the mechanisms involved are not well understood. We show that *brr6-1*, a mutant of the essential yeast envelope transmembrane protein Brr6p, impairs normal positioning and expression of the *PAB1* and *FUR4-GAL1,10,7* loci. Similarly, expression of a dominant negative nucleoplasmic Brr6 fragment in wild-type cells reproduced many of the *brr6-1* effects. Histone chromatin immunoprecipitation (ChIP) experiments showed decreased acetylation at the key histone H4K16 residue in the *FUR4-GAL1,10,7* region in *brr6-1*. Importantly, blocking deacetylation significantly suppressed selected *brr6-1* phenotypes. ChIPseq with FLAG-tagged Brr6 fragments showed enrichment at *FUR4* and several other genes that showed striking changes in *brr6-1* RNAseq data. These associations depended on a Brr6 putative zinc finger domain. Importantly, artificially tethering the *GAL1* locus to the envelope suppressed the *brr6-1* effects on *GAL1* and *FUR4* expression and increased H4K16 acetylation between *GAL1* and *FUR4* in the mutant. Together these results argue that Brr6 interacts with chromatin, helping to maintain normal chromatin architecture and transcriptional regulation of certain loci at the nuclear envelope.**

Monitoring Editor
Tom Misteli
National Cancer Institute, NIH

Received: Apr 26, 2018
Revised: Jul 30, 2018
Accepted: Aug 17, 2018

INTRODUCTION

Transcriptional regulation is intimately linked to dynamic spatial organization of genes within the nucleus (reviewed in Rajapakse and Groudine [2011], Zimmer and Fabre [2011], and Taddei and Gasser [2012]) and the nuclear envelope has emerged as an important organizing entity in chromatin architecture and regulation (reviewed in Steglich *et al.* [2013], Stancheva and Schirmer [2014], and Czapiewski *et al.* [2016]). Mutations in nuclear envelope transmembrane (NET) protein genes are linked to numerous human genetic diseases and certain cancers (reviewed in Stancheva and Schirmer [2014], Wong *et al.* [2014], Janin *et al.* [2017]), underscoring the importance of understanding the role of NET proteins in transcriptional regulation.

Correlation between localization of certain genes to the nuclear periphery and either activation or silencing has been demonstrated from yeast to mammals and artificially breaking or creating a tether to the nuclear envelope affects gene activity in some cases (e.g., Andrulis *et al.* [1998], Galy *et al.* [2000], Feuerbach *et al.* [2002], Taddei *et al.* [2006]). Work in the yeast system has been instrumental in identifying various mechanisms by which genes are targeted to the nuclear envelope including DNA zip codes and transcription factor binding (reviewed in Brickner [2017]). However, in spite of recent progress, the mechanistic relationship between envelope association and gene regulation is not well understood. The complexities of this problem are well exemplified by the yeast *GAL1,10,7* gene cluster required for galactose utilization in budding yeast. The *GAL1-10* locus relocates to the envelope upon galactose induction and transcriptional activation is necessary though not sufficient for localization (Cabal *et al.*, 2006). However, localization to the envelope is not required for activation and has been proposed instead to allow for rapid repression following inactivation (Green *et al.*, 2012). Two DNA zip codes, GRS4 and GRS5, present upstream of *GAL1* have been shown to target the *GAL* locus to the envelope, but only GRS4 affects activation, raising further questions regarding the function of envelope association (Brickner *et al.*, 2017).

This article was published online ahead of print in MBoC in Press (http://www.molbiolcell.org/cgi/doi/10.1091/mbc.E18-04-0258) on August 22, 2018.

*Address correspondence to: Christine Guthrie (christineguthrie@gmail.com) or Anne de Bruyn Kops (annedebk@gmail.com).

Abbreviations used: ChIP, chromatin immunopreciptitation; ChIPseq, ChIP sequencing; NET, nuclear envelope transmembrane; ncRNA, noncoding RNA; ORF, open reading frame; RNAseq, RNA sequencing; RT-qPCR, quantitative reverse transcription PCR; smFISH, single-molecule fluorescence in situ hybridization; UTR, untranslated region.

Positioning genes in subcompartments such as the nuclear periphery, rich in chromatin modifying, transcription and processing factors, is thought to contribute to regulation (reviewed in Rajapakse and Groudine [2011], Zimmer and Fabre [2011], Taddei and Gasser [2012]). However, genes are often closely spaced in yeast such that recruitment of one locus may expose an adjacent gene with different regulatory requirements to the same general environment. Consistent with this idea, a recent study of *GAL* locus repositioning upon galactose induction showed that other loci distantly located on the same chromosome were also peripheralized (Dultz *et al.*, 2016). Even within the same locus, differential regulation is required to curtail the generation of deleterious noncoding RNA (ncRNA) transcription from bidirectional promoters (reviewed in Wei *et al.* [2011]). How these requirements intersect with recruitment of loci at the nuclear rim is not well understood.

At a mechanistic level, gene activity is regulated by various chromatin modifications, such as acetylation on histone tails, that determine access of transcription factors to the DNA (reviewed in Grunstein and Gasser [2013]). In particular, acetylation status of the histone H4K16 residue has emerged as an important determinant of chromatin compaction (Dorigo *et al.*, 2003; Shogren-Knaak *et al.*, 2006; Robinson *et al.*, 2008; Allahverdi *et al.*, 2011; Liu *et al.*, 2011; Zhang *et al.*, 2017), and deacetylation/acetylation at this residue has been proposed to act as a switch that controls the binding of regulatory proteins and chromatin remodelers (Millar *et al.*, 2004).

Chromatin modifications are also believed to play a part in targeting genes to the nuclear envelope in yeast and higher eukaryotes through various mechanisms (reviewed in Harr *et al.* [2016] and Brickner [2017]). For example, the yeast SAGA histone acetyl transferase (Cabal *et al.*, 2006; Luthra *et al.*, 2007) and the Rpd3(L) deacetylase (Randise-Hinchliff *et al.*, 2016) affect gene recruitment to the envelope by regulating association of transcription factors that interact with the nuclear pore complex (NPC). In addition, deacetylation at H4K16 provides a physical link between yeast telomeres and the envelope by promoting association of Sir silencing proteins that in turn bind to the NET protein Esc1 (Andrulis *et al.*, 2002; Taddei *et al.*, 2004; Oppikofer *et al.*, 2011; Laporte *et al.*, 2016).

A clearer understanding of gene regulation at the nuclear envelope will require greater insight into the role of chromatin modifications as well as the identification of the membrane components that mediate gene recruitment. Most attention has focused on NPC components in this regard (reviewed in Ptak *et al.* [2014] and Sood and Brickner [2014]); however, several yeast NETs besides Esc1 (Scs2 Mps3, Scr1, and Nur1) have also been found to interact with chromatin (Brickner and Walter, 2004; Bupp *et al.*, 2007; Grund *et al.*, 2008; Mekhail *et al.*, 2008). Here we demonstrate a previously unknown role for another NET protein, Brr6, in the recruitment of specific genes to the nuclear envelope, maintenance of appropriate H4K16 acetylation, and transcriptional regulation. We originally identified *BRR6* via isolation of the *brr6-1* allele in a dT50 in situ hybridization screen for cold-sensitive mRNA export mutants in *Saccharomyces cerevisiae*. We showed that Brr6 is a c-terminally anchored nuclear envelope integral membrane protein that is required for normal nuclear pore distribution but is not itself a nucleoporin (de Bruyn Kops and Guthrie [2001] and unpublished data). Brr6 also affects lipid homeostasis and NPC assembly in *S. cerevisiae* (Scarcelli *et al.*, 2007; Hodge *et al.*, 2010; Lone *et al.*, 2015) and spindle pole body insertion in *Schizosaccharomyces pombe* (Tamm *et al.*, 2011).

We show here that the *brr6-1* mutant 1) impairs positioning of the *PAB1* and *GAL1,10,7* loci to the nuclear envelope; 2) associates physically with specific genes, including *FUR4* located adjacent to *GAL1,10,7*; and 3) alters expression of the *GAL1,10,7* and *FUR4* genes as well as noncoding transcripts. We reproduce many of these effects in wild-type cells expressing a dominant-negative non–membrane-bound form of Brr6 in the nucleoplasm. Importantly, we link misregulation at *FUR4-GAL7* to hypoacetylation at H4K16 and show that artificial recruitment of the *GAL1* locus to the envelope overcomes *GAL1* and *FUR4* expression defects, concomitant with increased H4K16 acetylation in the region. Our results suggest that Brr6 helps recruit specific genes to the nuclear envelope, promoting appropriate differential regulation by enabling acetylation at H4K16.

RESULTS

We previously identified *brr6-1* in a dT50 in situ hybridization screen for mutants in *S. cerevisiae* that accumulated bulk mRNA in the nucleus (de Bruyn Kops and Guthrie, 2001). Our subsequent characterization showed that cells in which *BRR6* expression was shut off also accumulated mRNA in the nucleus (Supplemental Figure 1A). Notably, a nucleoplasmic form of Brr6 (the galactose-controlled P_{GAL}–NLS-Brr6N fragment lacking the membrane anchor and luminal portion) did not rescue a Δ*brr6* strain; instead, expression of the NLS-Brr6N fragment in wild-type cells was dominant negative and caused a bulk mRNA export defect, consistent with the fragment competing with the endogenous protein (Supplemental Figure 1, B–F). The *brr6-1* mutation is located in a putative zinc finger and a Brr6 fragment in which the zinc finger domain was deleted (P_{GAL}–NLS-Brr6ΔC4N) showed no effects on growth or export, pointing to the importance of this domain for Brr6 function.

Our earlier work showed that Brr6 is a c-terminally anchored nuclear envelope integral membrane protein that is required for normal nuclear pore distribution but is not itself a nucleoporin (de Bruyn Kops and Guthrie, 2001). The *brr6-1* mutant affects localization of nucleoporins comprising the cytoplasmic fibrils of the NPC (Scarcelli *et al.*, 2007; Hodge *et al.*, 2010) but most core nucleoporins and those comprising the nuclear basket structure important in RNA export are not strongly affected (Scarcelli *et al.* [2007], Hodge *et al.* [2010], and de Bruyn Kops [unpublished data]). Evidence suggests that the mutant affects NPC assembly but not stability (Scarcelli *et al.*, 2007) and *brr6-1* showed no effect on protein trafficking (de Bruyn Kops and Guthrie, 2001), consistent with a functional NPC. Thus, it has not been clear how Brr6 impacts mRNA export.

The *brr6-1* mutant impairs *PAB1* transcript levels, indirectly causing the bulk mRNA export defect

To better understand the nature of the *brr6-1* bulk mRNA export defect seen by dT50 in situ hybridization, we wanted to examine the localization of a specific mRNA. We chose the *PAB1* transcript because it is abundant and decreased Pab1GFP signal seen by fluorescence microscopy (Figure 1A) was consistent with a possible *PAB1* mRNA export defect. Interestingly, Pab1GFP signal in *brr6-1* showed high cell–cell variability in keeping with the incomplete penetrance of the bulk mRNA export defect (de Bruyn Kops and Guthrie, 2001). Flow cytometry experiments confirmed both the decreased Pab1GFP levels and increased cell–cell variance in *brr6-1* (Figure 1A). Decreased Pab1GFP levels were also observed on expression of the NLS-Brr6N but not the NLS-Brr6ΔC4N fragment (Figure 1B).

To determine whether *brr6-1* affected *PAB1* mRNA export, we used single-molecule fluorescence in situ hybridization (smFISH) to localize individual *PAB1GFP* mRNA molecules using an established probe mix against the *GFP* sequence (Abruzzi *et al.*, 2006) and methods developed by the Singer lab (Zenklusen and Singer, 2010). Wild-type cells grown at 30°C showed numerous *PAB1GFP* mRNA

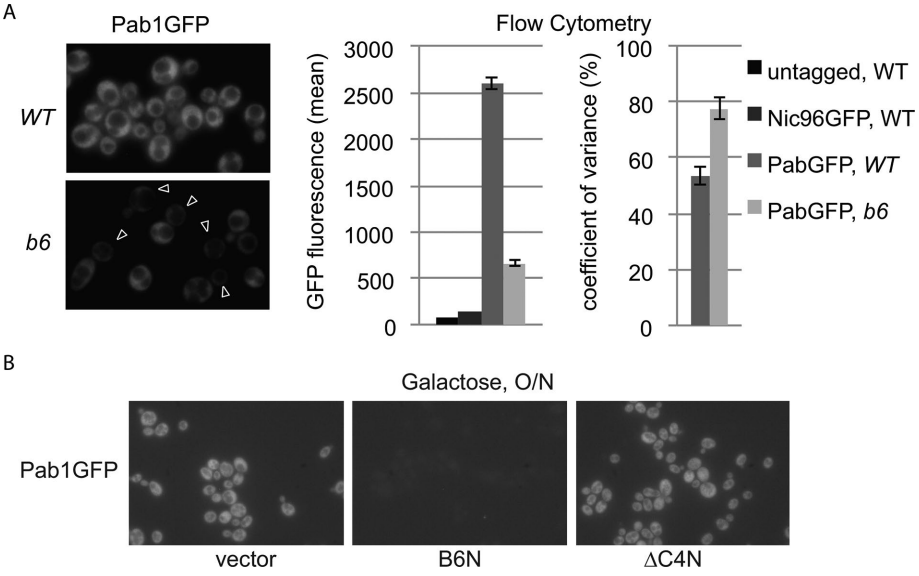

FIGURE 1: The *brr6-1* mutant and the NLS-Brr6N fragment impair *PAB1* expression. (A) Fluorescence microscopy localizing Pab1GFP in live isogenic WT (wild-type, yDBK398) and *b6* (*brr6-1*, yDBK399) cells. Arrowheads indicate cells with little Pab1GFP protein signal. Plots show quantitation of Pab1GFP levels by flow cytometry. (B) Pab1GFP in wild-type cells (W303) carrying empty vector (pJL602), *B6N* (pP_{GAL}_NLS-*BRR6*N-FLAG), or Δ*C4N* (pP_{GAL}_NLS-*brr6*Δ*C4*N-FLAG) grown in raffinose media then induced with galactose O/N.

molecules throughout the cell (Figure 2A). Staining of untagged cells showed no signal (Supplemental Figure S2), confirming that the probe detected *PAB1GFP* mRNA. *PAB1* mRNAs were also detected throughout the cell in the mutant. Interestingly, the *PAB1GFP* mRNA data mirrored the protein localization results with *brr6-1* cells showing reduced numbers of mRNAs relative to wild-type and high cell–cell variance (Figure 2A). Thus, we did not observe a defect in export of *PAB1*GFP mRNA in *brr6-1* even though nuclear accumulation of bulk mRNA had been detected in *brr6-1* by dT50 in situ hybridization. It is possible that the nuclear dT50 signal reflected mild decreases in export of many transcripts not detectable at the specific mRNA level.

The smFISH results suggested that reduced *PAB1* mRNA levels, rather than an export defect, are responsible for decreased Pab1 protein expression. To confirm the decrease in *PAB1* mRNA levels, we used quantitative reverse transcription PCR (RT-qPCR) to quantify *PAB1* transcripts in wild type and *brr6-1*. cDNAs were synthesized using a DN9 primer and quantified by qPCR using primers specific for the *PAB1* 5′ and 3′ open reading frame (ORF) regions. Results were normalized using a *Cryptococcus* RNA control added to each RT reaction (see *Materials and Methods*). The *brr6-1* cells grown at 30° C showed lower levels of *PAB1* transcript than wild type with both primer sets, and cells shifted to 16°C for 3 h showed stronger effects (Figure 2B). A similar effect was observed during a *BRR6* shutoff using a P_{GAL}–*BRR6* strain switched from galactose to glucose media (Figure 2C). These results confirmed that *BRR6* is required for normal *PAB1* transcript levels.

brr6-1 impairs positioning of *PAB1* and *GAL1-10* loci at the nuclear rim

The effects of the *brr6-1* mutation, the *BRR6* shut-off, and the NLS-Brr6N fragment on *PAB1* RNA and protein levels suggest a role for Brr6 in *PAB1* regulation. Because Brr6 is a nuclear envelope transmembrane protein and the regulation of some genes correlates with their recruitment to the nuclear envelope, we wondered whether the *PAB1* locus is recruited to the envelope. To examine this, we employed a commonly used method for visualizing the position of specific gene loci in individual cells in which a *LAC* operon tag (an approximately 14-kilobase-pair insert consisting of *LAC O* repeats and a marker [Rohner *et al.*, 2013]) is inserted near the gene of interest and localized in living cells by binding of LacI GFP to the operon repeats. Comparison of *PAB1* locus position in isogenic wild-type and *brr6-1* strains with a locus tag just upstream of the *PAB1* promoter (*LAC O:PAB1),* showed preferential positioning of the *PAB1* locus at the envelope in wild-type but not *brr6-1* cells (Figure 3A), indicating that *PAB1* is recruited to the envelope in a Brr6-dependent manner. The magnitude of this effect was comparable to *GAL1-10* locus positioning defects reported previously in various mRNA biogenesis mutants (Cabal *et al.*, 2006; Green *et al.*, 2012). Expression of the NLS-Brr6N fragment also caused decreased rim association of the *PAB1* locus compared with the NLS-Brr6ΔC4N fragment in cells grown in 2% raffinose/0.04% sucrose followed by induction with 2% galactose for 2 h (Figure 3B).

Interestingly, the *LAC O* cassette adjacent to the *PAB1* promoter in a *LAC O:PAB1* strain both restored Pab1GFP protein levels and overcame the bulk mRNA export defect (Supplemental Figure S3, A and B). We speculate that insertion of the large, repeat-rich tag substantially alters chromatin architecture in the region, affecting *PAB1* expression. Elimination of the export defect in *brr6-1 LAC O:PAB1* argues strongly that the bulk mRNA export phenotype in *brr6-1* stems from perturbed Pab1 protein levels, consistent with the known requirement for Pab1 in mRNA export (Brune *et al.*, 2005; Dunn *et al.*, 2005). Because the *LAC O:PAB1* insertion was identical in wild type and *brr6-1*, the decreased rim association seen in the mutant was not the result of the effects of the tag on *PAB1* expression. The *brr6-1* effects on *PAB1* expression were also independent of the tag as they were observed in untagged strains.

The *GAL1,10,7* gene cluster required for galactose utilization is among the most studied loci regulated at the envelope in budding yeast. Poor growth of the *brr6-1* mutant on galactose media (Figure 3C) suggested that Brr6 might also play a role in *GAL* gene expression. Therefore, we asked whether *brr6-1* also affected *GAL1-10* locus positioning using isogenic wild-type and *brr6-1* strains derived from crosses with a strain containing a *LAC O* tag inserted in the *GAL1-10* intergenic region (Schmid *et al.*, 2006). We saw no difference in *GAL1-10* locus position between wild-type and *brr6-1* cells in glucose. However, envelope recruitment in cells grown in 2% raffinose/0.04% sucrose and then induced with 2% galactose for 5 h was impaired in *brr6-1* (Figure 3D). These results show that the *brr6-1* mutation interferes with recruitment of both *PAB1* and *GAL1-10* loci to the nuclear envelope.

brr6-1 alters expression at the *GAL* locus

To examine the effect of *brr6-1* on expression of genes in the *GAL1,10,7* cluster, we compared transcripts produced in wild-type and *brr6-1* cells using whole genome RNA deep sequencing analysis (RNAseq). The mutant showed decreased transcript levels across the

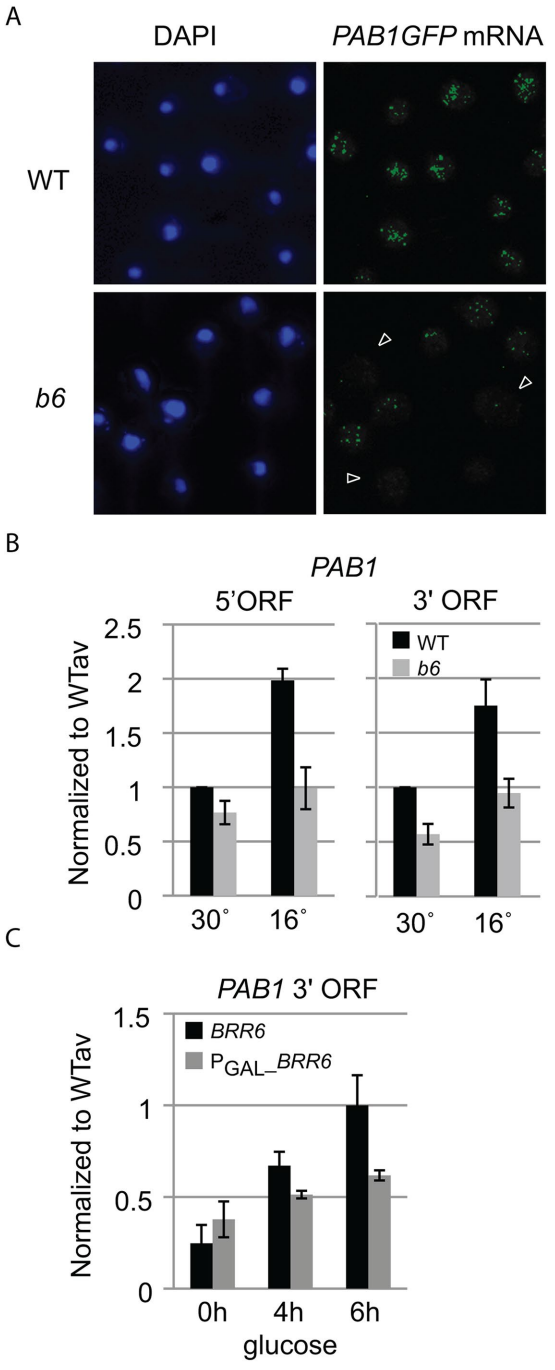

FIGURE 2: *brr6-1* decreases *PAB1* transcript levels. (A) Single-molecule FISH detecting *PAB1GFP* mRNA in fixed isogenic WT (wild-type, yDBK165) and *b6* (*brr6-1*, yDBK166) cells. Nucleus is detected by DAPI staining. Arrows indicate cells with little *PAB1*GFP RNA signal. Untagged control is shown in Supplemental Figure S2. (B) DN9 primed RT-qPCR detection of *PAB1* 5′ and 3′ ORF transcripts in total RNA prepared from WT (wild type, yDBK165) and *b6* (*brr6-1*, yDBK166) cells grown at 30°C or shifted for 3 h to 16°C. (C) RT-qPCR detection of *PAB1* 3′ transcripts from *BRR6* (yDBK155) and P_{GAL}*_BRR6* (yDBK192) cells following a time course of glucose repression. RT-qPCR data were normalized against a *Cryptococcus* RNA control (see *Materials and Methods*) and expressed relative to an averaged wild-type sample. Error bars (SEM) reflect four biological replicates.

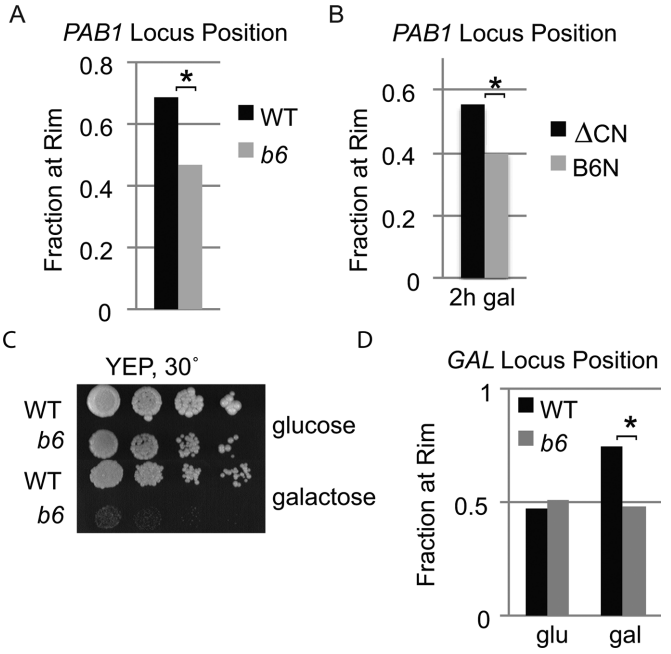

FIGURE 3: *brr6-1* and the NLS-Brr6N fragment impair *PAB1* and *GAL1-10* locus positioning. (A, B) Locus positioning assay showing fraction of *PAB1* locus at the nuclear rim in homozygous diploid *LAC O:PAB1* cells (A) WT (wild type, yDBK523) vs. *b6* (*brr6-1*, yDBK524) and (B) wild-type (W303) cells carrying B6N (pP_{GAL}_NLS-*BRR6N*) or ΔC4 (pP_{GAL}_NLS-*brr6ΔC4N*) fragment constructs. (C) Growth of WT (wild-type, yDBK165) and *b6* (*brr6-1*, yDBK166) strains on YEP media containing glucose or galactose. (D) Locus positioning assay for *GAL1-10* locus in homozygous diploid *LAC O:GAL1* cells (WT [wild type, yDBK535] vs. *b6* [*brr6-1*, yDBK536]). Asterisks indicate *p* value $\leq 6 \times 10^{-5}$.

GAL1,10,7 gene cluster compared with wild type (Figure 4A and Supplemental Table S3). Notably, the expression changes for the *GAL* transcripts were on the order of twofold decreases, similar to that observed for *PAB1* (Figure 2 and Supplemental Table S3); yet the *brr6-1* mutant showed a dramatic growth defect on galactose media in the absence of other carbon sources (Figure 3). We think that the explanation for this can be found in the *PAB1* mRNA and protein localization experiments as well as the flow cytometry, each of which indicates high cell-to-cell variance. In both the mRNA and protein localization experiments, some cells appear mostly normal, while others are severely impacted. Such nonpenetrant phenotypes can indicate stochasticity in underlying processes (e.g., Raj *et al.* [2010] and reviewed in Kærn *et al.* [2005] and Neems and Kosak [2010]). The *brr6-1* mutation is a conservative Arg to Lys change at the tip of a putative zinc finger. This mutation is unlikely to disrupt the structure of the zinc finger but could make its interactions less robust. Stochastic, transient protein binding events involved in gene expression can be stabilized by additional interactions during the formation of functional entities (reviewed in Misteli [2001]). Weak binding of the Brr6-1 mutant protein may decrease the opportunity for stable associations necessary for *GAL* and *PAB1* expression. A complete inhibition of *GAL* expression in 50% of cells would give a modest twofold effect in bulk assays such as RT-qPCR and RNAseq yet would represent an important disruption of function. Loss of *GAL* function in an additional 50% of cells during each subsequent cell cycle could result in the dramatic growth defect observed on galactose plates.

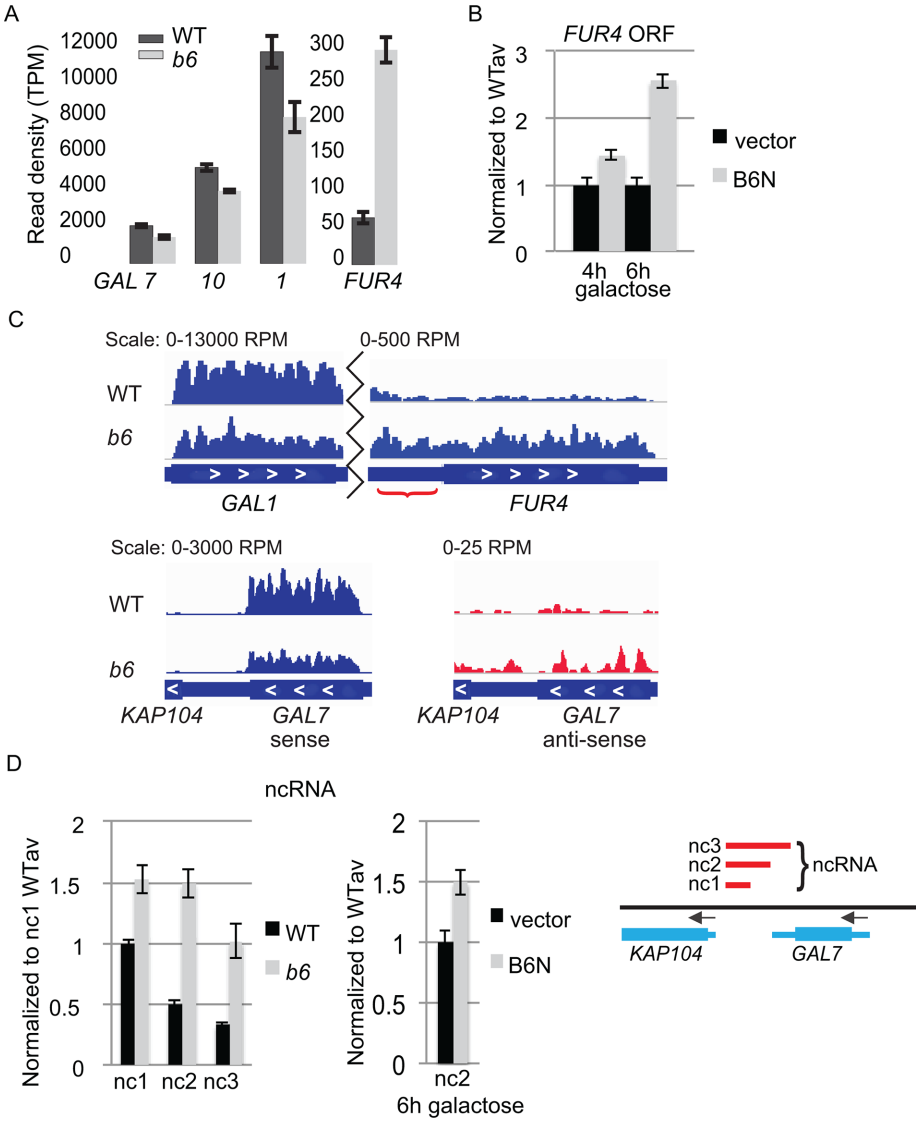

FIGURE 4: *brr6-1* and the NLS-Brr6N fragment perturb coding and noncoding transcription at the *FUR4-GAL1,10,7* gene region. (A) RNAseq results comparing transcript levels (read density [transcripts per million, TPM]) for *GAL7*, *GAL10*, *GAL1*, and *FUR4* in WT (wild type, yPH399) vs. *b6* (*brr6-1*, yDBK168). (B) RT-qPCR measurement of *FUR4* ORF transcripts in wild-type cells (W303) carrying vector (pJL602) vs. the B6N (pP_{GAL}NLS-*BRR6N*) construct. (C) Bar plot of RPM-normalized aligned sense (blue) reads for *GAL1* and *FUR4* coding and intergenic regions (red bracket) and sense and antisense (red) reads for *GAL7* (representative replicates). (D) DN9 primed RT-qPCR of ncRNA (nc1, 2, and 3) transcripts in WT (wild-type, yDBK165) and *b6* (*brr6-1*, yDBK166) cells (left) and the nc2 transcript in wild-type cells (W303) carrying vector (pJL602) vs. the B6N (pP_{GAL}NLS-*BRR6N*) construct (middle). Amplicons (*GAL* nc1-3) are indicated by red bars in the region from *KAP104* to *GAL7* (right). qPCR data were normalized and expressed as in Figure 2. Error bars (SEM) reflect ≥3 biological replicates.

Interestingly, regulation of the *FUR4* gene immediately adjacent to *GAL1* was also altered in the RNAseq data but showed increased read density. The increase in *FUR4* transcript levels was also observed by RT-qPCR following expression of the *GAL* promoter-driven NLS-Brr6N fragment in wild-type cells (Figure 4B). We did not see changes in *GAL* gene transcript levels in the NLS-Brr6N samples (unpublished data). It may be that twofold decreases in transcription are difficult to detect on top of high levels of *GAL* transcripts transcribed before the NLS-Brr6N protein fragment accumulated. Although *GAL* transcript half-lives are known to be short in wild-type cells (Bennett *et al.*, 2008; Munchel *et al.*, 2011), we do not know whether NLS-Brr6N induction affects RNA turnover rates. Alternatively, the effect of Brr6 on *FUR4* and *GAL* gene expression may be inherently different in ways we do not currently understand.

Interestingly, the RNAseq data also showed increased transcription in the *GAL1-FUR4* intergenic region (Figure 4C, bracket), indicating that there is misregulation in noncoding as well as coding regions. Similarly, increased antisense reads in the *GAL7-KAP104* region suggested that aberrant noncoding transcription may also occur on the other side of the *GAL1,10,7* locus (Figure 4C). The antisense read density was too low to be included in the DESeq2 statistical analyses (50 reads per kilobase cutoff); therefore we carried out RT-qPCR to confirm whether aberrant ncRNA is detectable downstream of *GAL7* using a primer set (nc1) located in the *KAP104-GAL7* intervening sequence. We detected antisense RNA at low levels in both mutant and wild-type cells following but not prior to a 2 h galactose induction, with levels in *brr6-1* being slightly higher than in wild type (Supplemental Figure 4). To ask whether this RNA extended further towards *GAL7*, we increased the amplicon size by moving the *GAL7* proximal primer to the middle (primer nc2) and beginning (primer nc3) of the *GAL7* 3′ untranslated region (UTR), respectively. With both of these primers, we detected >2× higher levels of antisense transcript in RNA from *brr6-1* than from wild type (Figure 4D). Thus, it appears that an ncRNA transcript is produced on galactose induction that is restricted more effectively in wild type than in mutant. Increased levels of the nc2 ncRNA were also detected following NLS-Brr6N fragment induction (Figure 4D). Together, these results show that Brr6 is required for normal transcript levels at and around the *GAL1,10,7* locus.

Histone H4 hypoacetylation underlies the *brr6-1* transcription defects

Transcription of both sense and antisense RNAs is regulated by various histone modifications such as acetylation on histone tails (reviewed Grunstein and Gasser [2013]). Hence, we wondered whether histone acetylation patterns in the *GAL7* region were altered in *brr6-1*. We examined histone H3 and H4 acetylation in the *GAL7* region using chromatin immunoprecipitation (ChIP). Acetylation relative to total H3 and H4 was determined using qPCR primer sets in the region spanning the *GAL10* 3′ ORF to the *GAL7* 3′UTR. Multiple lysine residues on both H3 and H4 are known to be acetylated; therefore we initially used pan-acetyl antibodies recognizing all of these marks. In addition, we included samples from a *brr6-1/Δhda1* double mutant because the *HDA1* histone deacetylase (HDAC) has been linked to regulation of the *GAL* gene cluster (Wu *et al.*, 2001;

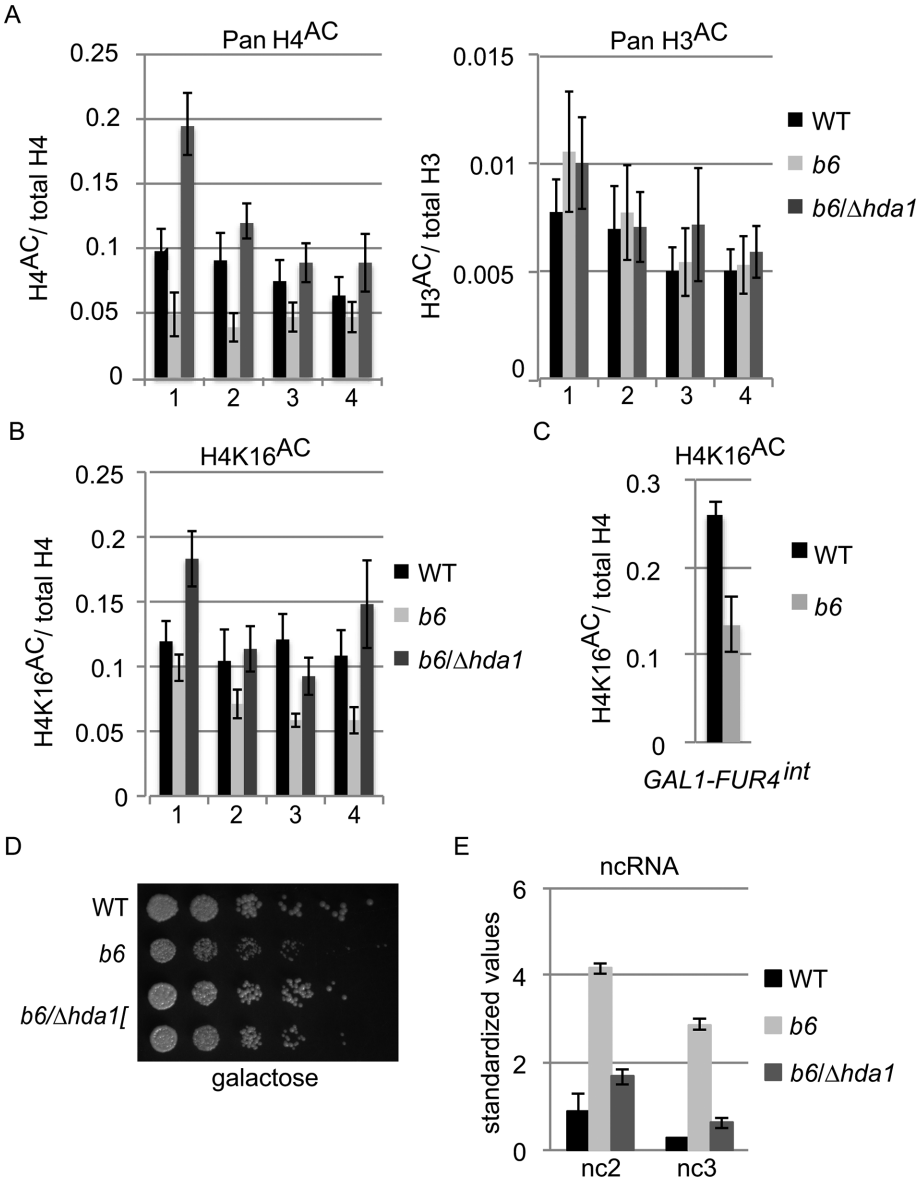

FIGURE 5: Aberrant transcription at *FUR4* and *GAL7* correlates with hypoacetylation at histone H4K16. (A, B) ChIP ratios of (A) pan-acetylated histone H4/total H4 pan-acetylated histone H3/total H3, and (B) lysine 16–acetylated H4 in WT (wild type, yDBK165), *b6* (*brr6-1*, yDBK166), and *b6/Δhda1* (*brr6-1/Δhda1*, yDBK169) cells following 2 h galactose induction. DNA was amplified using primer sets #1-4: #1-*GAL10* 3′ ORF, #2-*GAL7* 5′ ORF, #3-*GAL7* 3′ ORF, and #4-*GAL7* 3′ UTR. Total H4 and H3 values were normalized against WT prior to calculation of ratios. All antibody ChIP levels were >10× above mock ChIP. Error bars (SEM) reflect average of four biological replicates. (C) ChIP ratios of lysine 16–acetylated H4 amplified with primers for the *GAL1-FUR4* intergenic region. (D) Growth of WT (wild type, yDBK165), *b6* (*brr6-1*, yDBK166), and *b6/Δhda1* (*brr6-1/Δhda1*, yDBK169) double mutants on YEP +2% galactose, 0.04% sucrose at 30°C. (E) DN9 RT-qPCR detection of *GAL* ncRNA (nc2 and nc3) transcripts in WT, *b6*, and *b6/Δhda1* following galactose induction for 2 h at 30°C. qPCR data were normalized as in Figure 1. Error bars (SEM) reflect ≥3 biological replicates.

Houseley *et al.*, 2008). We observed hypoacetylation of H4 with all four primer sets in *brr6-1* (Figure 5A). In contrast, we saw no difference in H3 acetylation between wild type and *brr6-1*. Pan H4 acetylation returned to wild-type levels in the *brr6-1/Δhda1* double mutant; this was somewhat surprising given the reported specificity of Hda1 for histones H2A, H2B, and H3 (Wu *et al.*, 2001). However, HDACs show significant functional overlap and also deacetylate many nonhistone proteins in various cell processes, including chromatin dynamics (reviewed in Ekwall [2005] and Glozak *et al.* [2005]), that could affect activity of either histone acetylases (HATs) or HDACs. Detailed studies of the four acetylated lysines in H4 (K5, 8, 12, and 16) have shown that H4K5, 8 and 12 behave similarly in gene regulation while the functions of K16 appears to be distinct from those of the other residues (Millar *et al.*, 2004). Therefore, we also carried out ChIP with antibodies specific for acetylated H4K16. In this case, *brr6-1* showed marked hypoacetylation of the *GAL7* ORF and 3′ UTR but not the *GAL10* 3′ ORF (Figure 5B); this effect was reversed in the *brr6-1/Δhda1* double mutant. Similarly, we observed a decrease in H4K16 acetylation in the *GAL1-FUR4* intergenic region where increased noncoding transcription was also evident (Figure 5C).

Aberrant H4K16 deacetylation could readily explain the altered transcript levels in the *FUR4-GAL1,10,7* region seen in both *brr6-1* and following NLS-Brr6N fragment expression. Deletion of *HDA1* restored acetylation of H4K16 in *brr6-1* (Figure 5B); therefore, we examined the impact of *Δhda1* on selected *brr6-1* phenotypes (impaired growth on galactose media and the aberrant ncRNA downstream of *GAL7*). To examine the growth of the double mutant, cells were grown in 2% raffinose/0.04% sucrose and plated on 2% galactose/0.04% sucrose media. The small amount of sucrose improves growth of wild type and mutant in raffinose and galactose media, decreasing the extreme sickness of *brr6-1* seen on galactose alone (Figure 3) while still allowing detection of a significant growth defect. The *brr6-1/Δhda1* mutant showed substantial suppression of the *brr6-1* growth defect at 30°C (Figure 5D), consistent with restored *GAL* gene expression. The *brr6-1/Δhda1* strain also showed much less of the extended *GAL7* ncRNA than *brr6-1* alone (Figure 5E); thus, these *brr6-1* effects are significantly decreased when H4K16 acetylation is restored in *brr6-1/Δhda1*. These results indicate that the misregulation in the *GAL7* region is caused in part by altered H4K16 acetylation.

RNAseq analysis revealed genomewide transcriptional changes and CHIII disomy in *brr6-1*

In addition to changes in the *FUR4-GAL1,10,7* region, analysis of the RNAseq data showed that expression at 809 ORFs and 168 antisense transcripts was significantly ($p < 0.01$) decreased or increased ≥1.5× in *brr6-1* grown in galactose (Figure 6A and Supplemental Table S3; see Supplemental Table S4 for gene expression changes in glucose). To see how these changes were distributed throughout the genome, we mapped the Log2-fold changes to the midpoint of

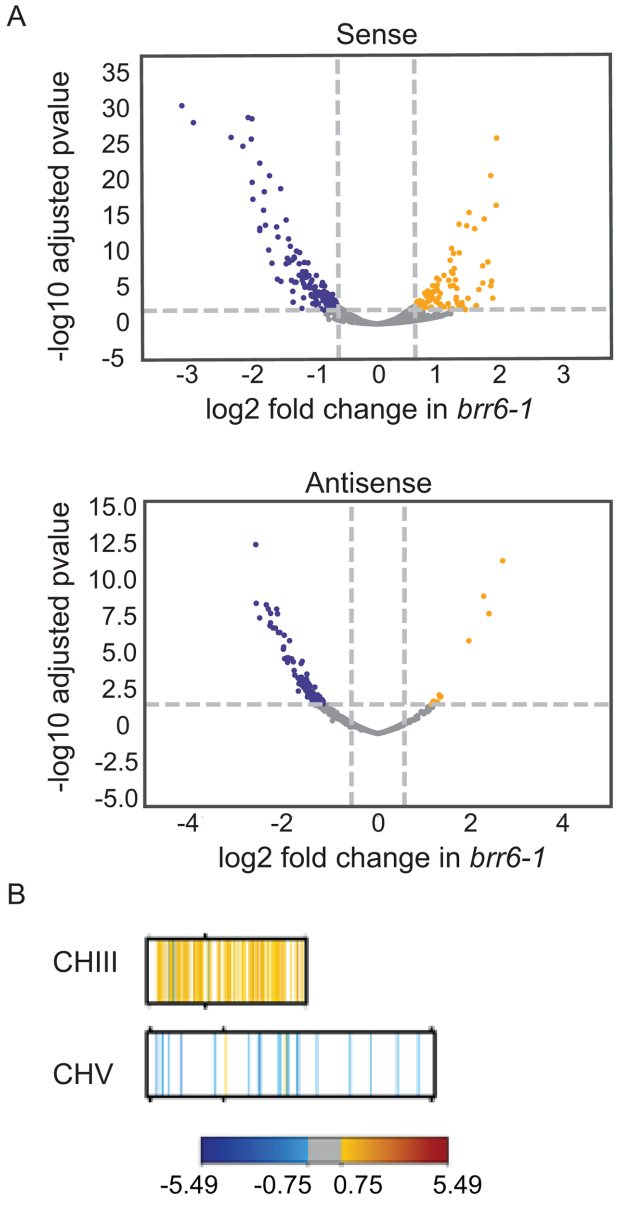

FIGURE 6: RNAseq analysis detects genomewide expression changes and CHIII disomy. (A) Volcano plots showing distribution of fold sense and anti-sense changes and adjusted *p* values in *brr6-1*(yDBK168) relative to wild-type (yPH399) cells following 2 h galactose induction (blue, fold decreases; yellow, fold increases; gray, changes between ± 0.75 log2 fold). Genes showing significant changes in galactose and glucose are listed in Supplemental Tables 3 and 4. (B) Mapping of genes showing altered sense reads in *brr6-1* (galactose) along CHIII and CHV (for other chromosomes and glucose results see Supplemental Figure S5, A and B).

each affected gene on the chromosomes (Figure 6B and Supplemental Figure S5). This showed that expression increased approximately twofold for many genes across CHIII but not other chromosomes (e.g., CHV), suggesting disomy at CHIII. Comparison of genomic DNA from wild-type cells and 2 separate *brr6-1* integrants confirmed stable disomy exclusively at CHIII (Supplemental Results and Supplemental Figure S6A).

The disomy raises the possibility that some of the expression changes result from altered CHIII gene copy number. However, GO term analysis of the genes affected in *brr6-1* (Supplemental Results and Supplemental Figure S6B) showed different enrichment patterns from those typically associated with disomy (Torres *et al.*, 2007), suggesting that some of the expression effects may relate to Brr6 function. We know that this is the case for the misregulation across the *FUR4-GAL1,10,7* region seen in *brr6-1* because increases in *FUR4* ORF and *GAL7* ncRNA transcript levels also occurred when the NLS-Brr6N fragment was transiently expressed in wild-type cells (Figure 4, B and D). In these experiments, the NLS-Brr6N fragment was transiently expressed following galactose induction for 2–12 h, making it unlikely that a large fraction of cells would have had time to generate a stable disomy. In fact, we have confirmed that CHIII is present in a single copy following overnight (O/N) induction of the NLS-Brr6N fragment (see below). The NLS-Brr6N fragment also duplicated the *brr6-1* effects on *PAB1* locus positioning and expression and the resulting mRNA export defect (Figures 1 and 3 and Supplemental Figure S1). Thus, the experiments with the NLS-Brr6N fragment confirm that Brr6 plays a role in regulation of both the *FUR4-GAL1,10,7*, and *PAB1* loci at the nuclear envelope.

The NLS-Brr6 fragment interacts physically with specific genes

Because *brr6-1* and the NLS-Brr6N fragment affect both recruitment of loci to the envelope and transcriptional regulation, we wondered whether Brr6 associates with chromatin. We attempted to carry out ChIP with Brr6 but encountered prohibitively low immunoprecipitation efficiencies, as is frequently the case with integral membrane proteins. The FLAG-tagged nucleoplasmic versions of the Brr6 fragments provided an alternative means of testing for physical interactions between Brr6 and chromatin. We carried out ChIPseq experiments using W303α cells carrying the pP_{GAL}_NLS-Brr6N-FLAG or pP_{GAL}_NLSBrr6ΔC4N-FLAG constructs or the empty vector grown O/N in galactose. qPCR of the DNA libraries confirmed the absence of CHIII disomy in the P_{GAL}_NLS-Brr6N-FLAG fragment strain (Supplemental Figure 7). Using a sliding window analysis (see *Materials and Methods*), we identified a small set of genes showing >2x enrichment in the NLS-Brr6N ChIP sample compared with vector (Figure 7A).

Of particular interest, the set included the *FUR4* gene located adjacent to the *GAL1*,7,10 locus. The NLS-Brr6ΔC4N fragment showed no enrichment at *FUR4* (Figure 7A), indicating that this effect was dependent on the Brr6 putative zinc finger. We were unable to determine whether the *GAL1,10,7* genes interacted with Brr6 because the nonspecific background (signal in vector sample) over the *GAL1,10,7* ORFs was very high (Figure 7B). A similar high background was observed over the *PAB1* ORF as well as the ORFs of the adjacent high-affinity glucose importer genes *HXT6* and *HXT7*. NLS-Brr6N-specific association evident in the *HXT6-7* intergenic region indicated a physical link between these genes and Brr6; however, the data did not reveal whether *PAB1* also associates. The high background over these ORFs was not a general feature of the ChIP data set and may reflect chromatin characteristics stemming from intense transcriptional activity as the *GAL1,7,10* and *HXT6,7* are induced in galactose and low glucose conditions respectively and *PAB1* is constituitively highly expressed.

The ability of the NLS-Brr6N fragment to both associate with *FUR4* and alter its expression (Figure 4) suggests that physical association with Brr6 may play a role in *FUR4* regulation. Several other gene regions showing NLS-Brr6N zinc finger-dependent enrichment also exhibited significant expression changes in *brr6-1* in galactose, suggesting that association with Brr6 may also contribute to their regulation. These included the *HXT7* and *HXT6* genes and the heat shock gene *HSP30* that are induced under conditions of limited glucose; notably, different expression effects were observed for

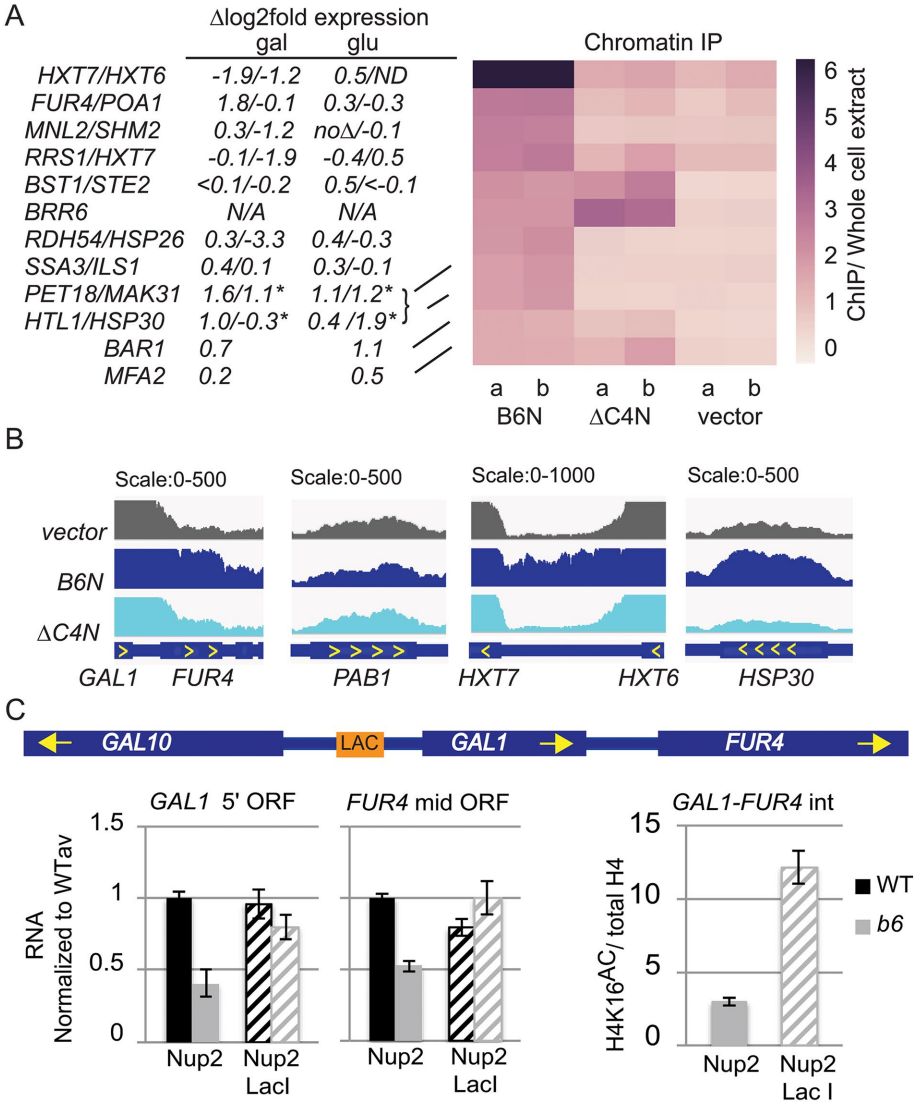

FIGURE 7: The NLS-Brr6N fragment associates with chromatin at *FUR4* and several glucose- and heatshock-responsive genes. (A) Right: Heatmap of the average read density (RPKM, ChIP normalized to whole cell extract) of Brr6 binding sites in ChIP samples from W303 cells carrying vector (pJL602), B6N (pP$_{GAL}$_NLS-*BRR6*N-FLAG), or ΔC4N (pP$_{GAL}$_NLS-*brr6ΔC4*N-FLAG) prepared following O/N galactose induction (two biological replicates). Regions of Brr6 binding were identified by sliding window (see *Materials and Methods*). Only regions with at least 1.5-fold ChIP/WCE are shown. Values are shown in Supplemental Table S5. qPCR confirming absence of CHIII disomy following B6N expression is shown in Supplemental Figure S7. (A) Left, changes in expression in *brr6-1* obtained by RNAseq analysis are shown for associated genes (*genes on CHIII not affected by *brr6-1* are predicted to show Δlog2 ≈ 1 expression changes due to disomy). (B) Bar plot of RPKM-normalized reads enriched in vector (pJL602), B6N (pP$_{GAL}$_NLS-*BRR6*N-FLAG), or ΔC4N (pP$_{GAL}$_NLS-*brr6ΔC4*N-FLAG) samples showing *GAL1-FUR4, PAB1,* and *HXT7-HXT6* and *HSP30*. (C) Left: RT-qPCR analyses of *GAL1* 5′ ORF and *FUR4* mid-ORF transcript levels in cells carrying a *LAC O* tag upstream of *GAL1* (see schematic) and either Nup2 and Nup2-Lac I *URA3*-marked constructs. (C) Right, comparison of H4K16 acetylation in the *FUR4-GAL1* intergenic region *brr6-1* cells carrying the *LAC O* tag and the Nup2 vs. Nup2-Lac I construct. Error bars (SEM) reflect three biological replicates.

these genes in galactose versus glucose (Figure 7A). Another heat-shock protein, *HSP26,* also showed both association and expression effects. *BRR6* itself was enriched in the fragment samples relative to the vector control; however, this reflected increased copy number from the plasmids encoding the Brr6 fragments, as indicated by the fact that the transmembrane and luminal portions of the sequence that are absent in the fragment constructs were not enriched (unpublished data). The ChIP results show that the NLS-Brr6N fragment associates physically with a small set of genes, including *FUR4*.

Together, the effect of *brr6-1* and the NLS-Brr6N fragment on recruitment of the *GAL* locus to the envelope and the *FUR4* ChIP result, along with the H4K16 acetylation and expression defects (Figures 4 and 5), raise the possibility that Brr6 performs a gene tethering function necessary for appropriate acetylation and regulation in this region. To test this idea, we asked whether artificially tethering the *GAL1* locus to the NPC could overcome the acetylation and expression defects. We made use of an established tethering approach in which wild-type and *brr6-1* cells carried a *LAC O* tag upstream of *GAL1* and a URA+ construct expressing a Nup2-Lac I fusion protein or Nup2 alone. Cells were grown in 2% raffinose/0.04% sucrose media lacking uracil to retain the plasmids and assayed following a 2 h galactose induction. In the presence of untagged Nup2, *brr6-1* showed decreased expression of both *GAL1* and *FUR4* relative to wild type (Figure 7C). *FUR4* is a uracil importer that is expressed under low uracil growth conditions and repressed in rich media (Séron *et al.*, 1999); hence, the decreased expression shows that *brr6-1* impairs optimal expression in low uracil as well as preventing appropriate repression in rich media (Figure 4). Importantly, the Nup2-Lac I construct largely overcame the expression defects for both *GAL1* and *FUR4* (Figure 7C). This argues strongly that these effects stem from failed envelope recruitment of the *GAL1-FUR4* region in *brr6-1*. Comparison of H4K16 acetylation in *brr6-1* cells carrying the Nup2-Lac I construct versus Nup2 alone showed greatly increased acetylation in the presence of the Nup2-Lac I construct (Figure 7C). Together, these results suggest that association of the *GAL-FUR4* region with the NPC promotes H4K16 acetylation and that artificial recruitment substitutes for a Brr6 tethering function needed for appropriate *GAL1* and *FUR4* regulation.

DISCUSSION

Our results showed that *brr6-1* impairs *PAB1* transcript levels (Figure 2) and disrupts *PAB1* and *GAL1-10* locus positioning (Figure 3), suggesting a role for Brr6 in controlling gene expression at the nuclear envelope. RNAseq analysis revealed changes in both coding and noncoding transcript levels across the *FUR4-GAL1,10,7* region (Figure 4 and Supplemental Table S3) and at numerous other genes (Figure 6). The discovery that *brr6-1* is disomic for CHIII raised the possibility that some of these effects stemmed from increased copy number of CHIII genes. However,

disomy was not present in wild-type cells where the NLS-Brr6N fragment was expressed (Supplemental Figure S7). Therefore, we were able to use the NLS-Brr6N fragment to link many of the *brr6-1* effects at the *PAB1* and *FUR4-GAL1,10,7* loci to Brr6 function, including the following: 1) decreased *PAB1* expression (Figure 1), 2) defective *PAB1* locus positioning (Figure 3), and 3) expression changes across the *FUR4-GAL1-10* region (Figure 4). Together with our ChIPseq results showing zinc finger-dependent association of the NLS-Brr6N fragment with the *FUR4* gene and the ability of an artificial NPC tether to overcome *GAL1* and *FUR4* expression effects in *brr6-1* (Figure 7), these results argue that Brr6 functions as a tether, helping to recruit the *FUR4* gene region to the envelope to ensure appropriate regulation.

Tethering via Brr6 promotes appropriate H4K16 acetylation and expression in the *FUR4-GAL1,10,7* region

We observed altered expression of the *GAL1,10,7* and *FUR4* ORFs and detected aberrant noncoding transcripts between *GAL1* and *FUR4* and between *GAL7* and *KAP104* (Figure 4) in *brr6-1*, consistent with general disruption of gene expression in the region. While it is possible that the expression changes reflect defects in other aspects of mRNA metabolism, the Histone H4K16 hypoacetylation seen in both of these locations in *brr6-1* (Figure 5) is consistent with effects on transcriptional regulation. Importantly, the *brr6-1* growth and *GAL7* ncRNA defects were substantially suppressed when H4K16 acetylation was restored in the Δ*hda1*/*brr6-1* double mutant (Figure 5), showing that these defects were caused at least in part by histone deacetylation at H4K16.

The ectopically expressed P_{GAL}_NLS-Brr6N fragment caused a dominant negative growth defect (Supplemental Figure S1) and recapitulated *brr6-1* expression changes across the *FUR4-GAL1,7,10* region, increasing both *FUR4* ORF and *GAL7* ncRNA transcript levels in rich media (Figure 4). Although the presence of the *GAL* promoter in the expression construct precluded assaying the effect of the NLS-Brr6N fragment on *GAL* locus positioning, the effect of the fragment on *PAB1* locus positioning duplicated the *brr6-1* effect. The similarity between *brr6-1* and the nucleoplasmic Brr6N fragment phenotypes, suggests that the NLS-Brr6N fragment competes with membrane bound Brr6. The NLS-Brr6N fragment associated physically with the *FUR4* locus (Figure 7) and *GAL* locus positioning was disrupted in *brr6-1* (Figure 3), making it likely that membrane-bound Brr6 also interacts with the *FUR4* region. Together, the expression changes, positioning defects and ChIP results raised the possibility that tethering of this region to the envelope by Brr6 may affect expression near *FUR4*. Importantly, the expression of an artificial NPC-Lac I tether largely eliminated *GAL1* and *FUR4* expression defects in *brr6-1* and strikingly increased H4K16 acetylation in the *GAL1-FUR4* region. This result strongly suggests that the NPC-Lac I substituted for a Brr6 tethering function necessary for optimal *GAL1* and *FUR4* regulation.

H4K16 acetylation promoted by Brr6 may optimize expression of certain inducible genes

Acetylation/deacetylation of the histone H4K16 residue has been proposed to act as a switch for chromatin architecture by promoting binding of different effector complexes and determining chromatin compaction (Millar *et al.*, 2004). Numerous in vitro studies have provided evidence that H4K16 acetylation decreases compaction by reducing internucleosome interactions (Dorigo *et al.*, 2003; Shogren-Knaak *et al.*, 2006; Robinson *et al.*, 2008; Allahverdi *et al.*, 2011; Liu *et al.*, 2011; Zhang *et al.*, 2017). Although the role of H4K16 in chromatin compaction in vivo is not fully understood, H4K16 acetylation is correlated with polycomb chromatin puffs in *Drosophila* (Bone *et al.*, 1994) and deacetylation plays a key role in heterochromatin formation in yeast (reviewed in Millar *et al.* [2004]). In addition, a H4K16 histone acetyltransferase functions in X chromosome decondensation in *Drosophila* (Lau *et al.*, 2016). However, studies in mammalian cells failed to demonstrate a connection with linear chromatin compaction (Taylor *et al.*, 2013). Similarly, linear chromatin compaction near the *GAL* locus was not perturbed in living yeast following deletion of the SAGA histone acetylase GCN5 or in the presence of the histone-deacetylase inhibitor trichostatin A (TSA) (Dultz *et al.*, 2018); however, mutants in the TSA-resistant deacetylase Sir2 (Bernstein *et al.*, 2000) and the SAS histone acetylase complex responsible for the H4K16 acetylation in vivo (Shia *et al.*, 2005) were not examined in these studies.

Based on the effects of H4K16 acetylation on chromatin compaction in vitro and in some in vivo systems, an attractive model is that the tethering function of Brr6 promotes access to regulatory proteins by helping maintain appropriate H4K16-mediated compaction in the *FUR4-GAL* gene cluster and other Brr6-interacting genes. Alternatively, H4K16 acetylation could alter interaction of regulators independent of chromatin compaction. In either scenario, we predict that gene-specific transcriptional outcomes of tethering would depend on both the presence of binding sites for specific regulators in different genes as well as the levels of regulators under different environmental conditions.

The fact that *FUR4* locus is differentially regulated from the immediately adjacent *GAL1* gene is consistent with gene-specific consequences of gene recruitment. Both the *GAL1* and the *FUR4* promoters carry the Gal4-responsive activating sequence (UAS_{GAL}), yet the normal increase in *GAL1* expression in wild-type cells following galactose induction is approximately two orders of magnitude greater (Figure 4A). Differences in response to galactose among genes containing the UAS_{GAL}, are thought to be determined both by the number and affinity of UAS_{GAL} sequences that vary among genes (Lohr *et al.*, 1995) and by differences in chromosome architecture in genes carrying the UAS_{GAL} (reviewed in Traven *et al.* [2006]). In *brr6-1*, *FUR4* expression increases 3.5× relative to wild type in rich media while transcript levels from the adjacent *GAL1* gene decrease 1.7×, indicating opposing misregulation of the adjacent genes. *FUR4* expression is also tightly controlled by uracil levels (Séron *et al.*, 1999), leading to increased and decreased transcripts in conditions of low uracil and rich media, respectively. The opposite effects of *brr6-1* on *FUR4* transcript levels in uracil dropout (Figure 7) versus rich media (Figure 4) reinforces the idea that failed Brr6 tethering results in misregulation rather than consistently either aberrant activation or repression.

It is interesting that we detected interactions between the NLS-Brr6N fragment and only a few genes. This may reflect an inability of the fragment to consistently reproduce interactions of the native membrane-bound protein. However, it is striking that most of the regions detected in the NLS-Brr6N ChIP carry genes that are regulated in a particular context such as heatshock (HSP26, HSP30, SSA3), mating type *a* cells (STE2, BAR1, MFA2) or carbon source (HXT7, HXT6). It may be that Brr6 functions to recruit a very small set of highly regulated genes that require tight transcriptional regulation under specific inducing conditions.

Conclusion

A large body of information links nuclear envelope components with chromatin organization and transcriptional regulation. Histone modifications govern chromatin architecture, providing the mechanistic basis for eukaryotic transcriptional regulation. The current work

argues that the Brr6 nuclear membrane protein aids in the recruitment of specific genes to the envelope and that gene tethering may promote a H4K16 chromatin architectural switch that is key for fine-tuning regulation of inducible genes as well as for allowing individual control of adjacent genes with different regulatory requirements.

This work establishes Brr6 as a valuable model for understanding the relationship of the nuclear envelope to chromatin architecture and gene regulation.

MATERIALS AND METHODS

Strains and plasmids

The pP_{GAL}_NLS-*BRR6*N (pDBK101) and pP_{GAL}_NLS*brr6-1*N (pDBK105) constructs were made by inserting a PCR-generated NLS(MAPKKKRKV)-*BRR6* or -*brr6-1*(codons 2–158) sequence (lacking the c-terminal transmembrane domain and luminal portion) into the pJL602 CEN/ARS vector containing the *GAL10* promoter and a *LEU2* marker (gift from Joachim Li, University of California, San Francisco). The pP_{GAL}_NLS-*brr6*Δ*C4*N zinc finger deletion construct (pDBK103) was generated by replacing *BRR6* sequence encoding amino acids 96–124 with an in-frame ClaI/SpH1 cassette (ATCGATGC). The FLAG-tagged versions of the (pDBK102, pDBK104, and pDBK106) constructs were generated by inserting a FLAG tag (DYKDDDDK) fragment with stop codon with Spe1/SacII ends at the C-termini of the fragment coding sequences. The tagged and untagged constructs and pJL602 vector were transformed into a W303 wild-type strain. The NUP2 pRS316 construct was a gift from Jonathan Loeb and Gerald Fink, Massachusetts Institute of Technology. Sequence encoding the Lac I tag was inserted into the plasmid in frame to give the *NUP2-LACI* pRS316 construct.

Strains used in this study are listed in Supplemental Table S1. GFP:HIS3 tagged strains (*PAB1*, *NUP60*, *POM34*) used in strain generation were obtained from the O'Shea library (Huh *et al.*, 2003). *PAB1GFP* strains were generated by crossing *PAB1GFP:HIS3* with wild-type and mutant *BRR6* strains (yDBK164 and yDBK165). *LAC O:PAB1* strains were made by inserting *LAC O* repeats at nucleotide –260 with respect to the *PAB1* ORF in a wild-type s288C strain background (ATC20089) using a previously described *LAC O:LEU* cassette and marker replacement method (Rohner *et al.*, 2008). Haploid wild-type and mutant strains were obtained from a cross with a strain carrying unmarked *brr6-1* and Pom34GFP:HIS3 (s288C background). These were subsequently crossed with *BRR6:HIS:LEU*,*LACIGFP:HIS3* and *brr6-1:HIS3:LEU2*,*LACIGFP:HIS3* strains (W303 background) to obtain diploids used in positioning assays. *LAC O:GAL1* strains were made by crossing a wild-type strain carrying the *GAL1* locus tag and *LACIGFP:HIS3* (YGA133 [Schmid *et al.*, 2006]) with unmarked wild-type and *brr6-1* strains (W303 background). These were subsequently crossed against Δ*brr6::HIS3* strains covered by *BRR6* and *brr6-1* on *TRP1* plasmids and carrying *NUP60:GFP:HIS3* to give diploids used in positioning assays. Diploid *LAC O:GAL1* strains were sporulated to yield the haploid *LAC O:GAL1*, *BRR6* and *brr6-1*-unmarked strains without *LACIGFP:HIS3* used in Nup2-Lac I tethering experiments. A YPH399 strain carrying the *brr6-1* mutation (yDBK168) was made by targeted insertion of *brr6-1* into the BRR6 downstream sequence in the Δ*brr6::HIS3* deletion strain yDBK123 (de Bruyn Kops and Guthrie, 2001). The resulting strain carries the *brr6-1* allele and LEU2 marker flanked by Δ*brr6*::HIS3.

Growth assays

Strains were grown to saturation and then diluted identically prior to pinning on appropriate media: *BRR6* mutant and wild-type cells were grown in yeast extract peptone (YEP) raffinose media and tested for growth on plates containing 2% glucose or 2% galactose (Figure 3C and Supplemental Figure S1E) or 2% galactose/0.04% sucrose (Figure 5D) at 30°C. For experiments with wild-type cells carrying the Brr6 fragment constructs or empty vector, YEP was replaced with synthetic minimal media (SD–Leu) media (Supplemental Figure S1E).

Fluorescence microscopy, locus positioning assays, and in situ hybridization

Fluorescence microscopy was carried out using an Olympus BX60 microscope equipped with a 100× UPlanApo oil-immersion objective and Hi-Q DAPI, Hi-Q FITC, and Edow long-pass GFP and CY3 filters (Chroma Technologies) and *z*-axis controller and 24-bit black-and-white Photometrics Sensys charge-coupled device (CCD) camera. Images were collected and processed using iVision (v.4.0.0), BioVision Technologies. Cells for all microscopy experiments were grown to 0.25–0.5 OD_{600}.

PabGFP localization and locus positioning assays. Diploid cultures (5 ml) were grown in glucose media (YEPD) at 30°C, harvested by brief centrifugation and resuspended in 10–20 µl synthetic complete (SC) media prior to live imaging to decrease media fluorescence. Diploid cells carried the *LAC O* repeat tag integrated adjacent to the *PAB1* or *GAL1* locus and LacIGFP as well as either Nup60GFP or Pom34GFP to locate the nuclear envelope. Loci were detected as a bright spot of LacI GFP signal that was readily distinguishable from the dimmer nucleoporin signal. Having both locators tagged with GFP allowed scoring of Loci positions without filter registration concerns. Cells with in-focus loci were scored as rim or internal depending on whether they contacted the envelope signal. Fields were photographed sufficient to give $p \leq 0.00006$ using a two-tailed, pooled two-proportions Z-test appropriate for binomial data.

In situ hybridization. Localization of bulk poly A mRNA in fixed cells was carried out as previously described (de Bruyn Kops and Guthrie, 2001) using a digoxygenin-labeled dT50 probe. Staining with 4′,6-diamidine-2′-phenylindole dihydrochloride (DAPI) was used to identify the nucleus. Single-molecule FISH Localization of *PAB1GFP* mRNA was carried out according to methods developed by the Singer lab (Zenklusen and Singer, 2010). The GFP probe consisted of 4 AMC6-dT–modified 56mer oligonucleotides (OGM191-194[KD209-212]) identical to those used to detect GFP RNA sequences previously (Abruzzi *et al.*, 2006). The probe was conjugated to CY3 dye (GE Healthcare) according to manufacturer's instructions. Images are pseudo-colored maximal projections of z-series.

Flow cytometry

GFP tagged and untagged cells were grown at 30°C to 0.3–0.5 OD_{600} in SC media with 2% glucose. Signals in the FITC channel were recorded from 40,000 cells/sample without media change using a LSRII flow cytometer (BD Biosiences). Data were analyzed using FlowJo single-cell analysis software. Coefficient of variation is defined CV = SD/mean and displayed in percent.

RT-qPCR detection of transcripts

Cells were grown to mid–log phase in YEP media containing glucose or 2% raffinose/0.04% sucrose as appropriate. For *GAL* gene induction, galactose was added to a final concentration of 2% at designated times prior to harvesting. RNA was extracted using an established hot acid phenol protocol. Total 20 µg RNA was treated with RNase-free DNase (10 U; NEB), phenol-chloroform extracted, ethanol-precipitated, and measured by Nano-Drop (Thermo Scientific). DNased RNA (0.5 µg) was reverse transcribed using SuperscriptIII (Invitrogen) with a DN9 random primer. Because the full range of

BRR6 transcription targets is unknown, it was not possible to select a gene for use as an internal control for normalization. Instead reactions were doped with 0.5 µg DNased *Cryptococcus neoformins grubii* H99 RNA to control for variabilities in RT efficiency and recovery and transcript levels were normalized to the level of Crypto *PAB* (CNAG_04441). Control experiments established complete absence of cross-detection with *Saccharomyces* and *Cryptococcus* probes (unpublished data). qPCR was carried out with four technical replicates (see Supplemental Table S2 for primer sets). Transcript levels from a minimum of three cryptonormalized biological replicates were normalized to the average of a wild-type sample.

qPCR determination of chromosome number

Genomic DNA from cells grown to mid–log phase was prepared by bead-beating in phenol. DNA was treated with RNase, quantified by nanodrop, and diluted to 3 ng/ul. DNA (5 µl) was assayed by qPCR (three biological replicates) using primers specific for selected genes on each chromosome (Supplemental Table S2).

RNA deep sequencing (RNAseq)

Sequencing experiments were done in the YPH399 (S288C derivative) background rather than W303, because a completely assembled and annotated reference genome is available for S288C. Cells (*brr6-1* [yDBK168] and wild-type parent [YPH399], two biological replicates) were grown at 30°C in 2% glucose or in raffinose/0.04% sucrose YEP media followed by a 2-h galactose (2%) induction prior to harvesting in mid–log phase. RNA was isolated as for RT-qPCR (see above) and rRNA was removed using a Ribominus kit for yeast and concentration module (Invitrogen). RNA was cleaned and DNase treated using the RNA Clean and Concentrator Kit (Zymo Research). RNA quality was checked by bioanalyzer using the Agilent RNA 6000 Pico Kit. RNA libraries were prepared using a NEBNext Ultra Directional RNA Library Prep kit for Illumina (E7420) and standard NEB protocol for ribosome-depleted RNA. Libraries were size selected (200–400 base pairs) and quality checked by bioanalyzer using the Agilent High Sensitivity DNA Kit prior to multiplexing for Illumina sequencing (single end, 50-base-pair reads) on Hiseq 4000. Genes showing significant changes in expression in *brr6-1* are listed in Supplemental Tables S3 (galactose) and S4 (glucose).

RNAseq data analysis. Sequencing data (two biological replicates per genotype) were aligned to the S288C (parental strain for YPH399) genome (Fisk *et al*., 2006) using TopHat1 (Trapnell *et al*., 2009) using the following parameters: tophat1 –min-intron-length 20 –max-intron-length 2000 –max-multihits 2 –library-type fr-firststrand –segment-mismatches 3 –no-coverage-search –segment-length 20 –min-coverage-intron 10 –bowtie1. Alignments were sorted and indexed with SAMtools (Li *et al*., 2009), and bedgraph files were created with BEDTools (Quinlan, 2014). Reads in annotated transcripts were counted using HTseq-count (Anders *et al*., 2015) and differential expression was determined using DESeq2 (Love *et al*., 2014). Transcripts with a log2-fold change of greater than 0.75 or less than –0.75 and an adjusted *p* value of at most 0.01 were considered significantly changed. The log2-fold change threshold was chosen based on the differential expression of *GAL7* in the *brr6-1* mutant, which is deficient for growth on galactose. Antisense regions were defined by the boundaries of each annotated transcript plus 300 base pairs downstream of the stop codon. A cutoff of 50 reads per kilobase was used for antisense transcripts. The differential expression of RNA in the antisense region was analyzed as described above. Data from RNAseq and ChIPseq (see below) experiments are available in a GEO record (www.ncbi.nlm.nih.gov/geo/query/acc.cgi?acc=GSE113746). Expression changes for the affected transcripts were mapped to the midpoint position for each gene using chromosomal location data from the Yeast Genome Database (www.yeastgenome.org/).

Chromatin immunoprecipitation

Histone ChIP. Cells (DBK165 and DBK166) were grown to mid–log phase in YEP media containing 2% raffinose/0.04% sucrose and induced for 2 h by addition of 2% galactose. Cells (80 ml OD_{600} = 0.5 equivalents) were cross-linked for 15 min in 1% formaldehyde, quenched 15 min with 125 mM glycine, washed 2× in TBS, and resuspended in ChIP buffer (50 mM Tris [pH 7.4], 125 mM KCl, and 0.1% NP40) plus protease inhibitors (100 µM PMSF), Sigma and Complete protease tablet (Roche). Cells lysates generated by bead beating were bath sonicated 8 × 7.5 min and clarified by centrifugation 2 × 10 min at 2000 relative centrifugal force. Cell lysate (200 µl/sample) was incubated O/N at 4°C with 2–5 µl antibodies against histones: H3(Thermo PA5-16183), H4 (Millipore 04-858), acetylated H3(Millipore 06-599), pan-acetylated H4 (Millipore 06-866), and acetylated H4K16 (Millipore 07-329). Anti-histone and mock ChIP samples were incubated at 4°C for 3 h with 30 µl equilibrated protein A sepharose CL-4B beads (GE Healthcare) and then washed twice with 1 ml lysis buffer, once with 1 ml lysis buffer + 500 mM NaCl at 4°C, and once with Tris-EDTA buffer (TE) at room temperature. Beads were dissociated by heating 15 min at 65°C in 300 µl TE +1% SDS. Cross-links were reversed O/N at 65°C prior to proteinase K digestion and phenol chloroform extraction.

Brr6 fragment ChIPseq. Two biological replicates of wild-type cells carrying empty vector(pJL602), pP_{GAL}–NLS-*BRR6*N-FLAG, or pP_{GAL}–NLS-*brr6ΔC4N*-FLAG were grown to mid–log phase in YEP media containing 2% raffinose/0.04% sucrose, diluted into media containing 2% galactose/0.04% sucrose, and grown O/N. Cells (80 ml OD_{600} = 1.0) were cross-linked and lysates were generated as above. Extracts were sonicated 4 × 7.5 min in a bath sonicator, clarified, and incubated (350 µl/sample) O/N with 40 µl EZview Red anti-FLAG M2 affinity gel (Sigma) and washed as above. Cross-links were reversed and DNA libraries prepared as described in Inada *et al*. (2016). Library quality was confirmed by bioanalyzer using the Agilent High Sensitivity DNA Kit prior to multiplexing for Illumina sequencing (single end, 50-base-pair reads). Genes showing association with the NLS-Brr6N fragment are listed in Supplemental Table S5.

ChIP analysis methods. Adaptor was trimmed from the 3′ end of reads using Cutadapt (Martin, 2011). Trimmed reads (two biological replicates per genotype) were then aligned to the S288C genome (R64-2-1_20150113) using Bowtie (Langmead *et al*., 2009) with the following parameters: bowtie -p8 -v2 -M1 –best –un B6N_a_multi_un.fastq –max B6N_a_multi.fastq S288C_genome -q B6N_a_trim.fastq –sam B6N_a_multi.sam. Sequence alignment map (SAM) files were converted to binary alignment map (BAM) files, sorted, and indexed using SAMtools (Li *et al*., 2009). Alignment was done against S288C because the W303 genome is not fully assembled. Sorted and indexed BAM files were converted to bedgraph files using BEDTools (Quinlan, 2014). Bedgraph files were smoothed with a rolling mean of 100 base pairs using the Pandas Python package.

To identify regions of Brr6 binding, smoothed ChIP signal from the tagged samples (B6N) were divided by the signal from the untagged sample (PJL) after normalizing to the total number of aligned reads. A sliding window of 200 base pairs moving in increments of 20 base pairs was used to detect regions that had at least twofold

enrichment of signal in the tagged sample over the untagged sample. Regions that had at least 50% overlap in both replicates were selected. Only the overlapping portion of the region was considered for further analysis steps. Finally, the average read density (in RPKM) was calculated in each region of Brr6 binding for tagged and untagged and then normalized to the signal from the corresponding whole cell extract from that sample.

ACKNOWLEDGMENTS

This work was funded by National Institutes of Health–National Institute of General Medical Sciences grant 5R01GM021119 to C.G. C.G. was also supported by an American Cancer Society Professorship in Molecular Genetics. J.B. is supported by an American Cancer Society Post-doctoral Fellowship (127531-PF-15-050-01RMC). We thank Tristan Daifuku for computer programming assistance. We thank Daniel Zenklusen and Robert Singer for reagents and training with the single-molecule FISH assay. We thank Jonathan Loeb, Gerald Fink, and Joachim Li for gifts of plasmids. We are grateful to Kristin Patrick, Sarah Ledoux, Megan Mayerle, Michael Marvin, Kelly Nissen, Argenta Price, Christina Homer, Bassem Al-Sady, Jahan-Yar Parsa, Selim Boudoukha, Sandra Catania, Hiten Madhani, and David Tollervey for helpful discussions and comments on the manuscript.

REFERENCES

Abruzzi KC, Belostotsky DA, Chekanova JA, Dower K, Rosbash M (2006). 3'-end formation signals modulate the association of genes with the nuclear periphery as well as mRNP dot formation. EMBO J 25, 4253–4262.

Allahverdi A, Yang R, Korolev N, Fan Y, Davey CA, Liu C-F, Nordenskiöld L (2011). The effects of histone H4 tail acetylations on cation-induced chromatin folding and self-association. Nucleic Acids Res 39, 1680–1691.

Anders S, Pyl PT, Huber W (2015). HTSeq—a Python framework to work with high-throughput sequencing data. Bioinformatics 31, 166–169.

Andrulis ED, Neiman AM, Zappulla DC, Sternglanz R (1998). Perinuclear localization of chromatin facilitates transcriptional silencing. Nature 394, 592–595.

Andrulis ED, Zappulla DC, Ansari A, Perrod S, Laiosa CV, Gartenberg MR, Sternglanz R (2002). Esc1, a nuclear periphery protein required for Sir4-based plasmid anchoring and partitioning. Mol Cell Biol 22, 8292–8301.

Bennett MR, Pang WL, Ostroff NA, Baumgartner BL, Nayak S, Tsimring LS, Hasty J (2008). Metabolic gene regulation in a dynamically changing environment. Nature 454, 1119–1122.

Bernstein BE, Tong JK, Schreiber SL (2000). Genomewide studies of histone deacetylase function in yeast. Proc Natl Acad Sci USA 97, 13708–13713.

Bone JR, Lavender J, Richman R, Palmer MJ, Turner BM, Kuroda MI (1994). Acetylated histone H4 on the male X chromosome is associated with dosage compensation in Drosophila. Genes Dev 8, 96–104.

Brickner DG, Sood V, Tutucci E, Coukos R, Viets K, Singer RH, Brickner JH (2017). Subnuclear positioning and interchromosomal clustering of the GAL1-10 locus are controlled by separable, interdependent mechanisms. Mol Biol Cell 28, 2980–2993.

Brickner J (2017). Genetic and epigenetic control of the spatial organization of the genome. Mol Biol Cell 28, 364–369.

Brickner JH, Walter P (2004). Gene recruitment of the activated INO1 locus to the nuclear membrane. PLoS Biol 2, e342.

Brune C, Munchel SE, Fischer N, Podtelejnikov AV, Weis K (2005). Yeast poly(A)-binding protein Pab1 shuttles between the nucleus and the cytoplasm and functions in mRNA export. RNA 11, 517–531.

Bupp JM, Martin AE, Stensrud ES, Jaspersen SL (2007). Telomere anchoring at the nuclear periphery requires the budding yeast Sad1-UNC-84 domain protein Mps3. J Cell Biol 179, 845–854.

Cabal GG, Genovesio A, Rodriguez-Navarro S, Zimmer C, Gadal O, Lesne A, Buc H, Feuerbach-Fournier F, Olivo-Marin J-C, Hurt EC, Nehrbass U (2006). SAGA interacting factors confine sub-diffusion of transcribed genes to the nuclear envelope. Nature 441, 770–773.

Czapiewski R, Robson MI, Schirmer EC (2016). Anchoring a leviathan: how the nuclear membrane tethers the genome. Front Genet 7, 82.

de Bruyn Kops A, Guthrie C (2001). An essential nuclear envelope integral membrane protein, Brr6p, required for nuclear transport. EMBO J 20, 4183–4193.

Dorigo B, Schalch T, Bystricky K, Richmond TJ (2003). Chromatin fiber folding: requirement for the histone H4 N-terminal tail. J Mol Biol 327, 85–96.

Dultz E, Mancini R, Polles G, Vallotton P, Alber F, Weis K (2018). Quantitative imaging of chromatin decompaction in living cells. Mol Biol Cell 29, 1763–1777.

Dultz E, Tjong H, Weider E, Herzog M, Young B, Brune C, Müllner D, Loewen C, Alber F, Weis K (2016). Global reorganization of budding yeast chromosome conformation in different physiological conditions. J Cell Biol 212, 321–334.

Dunn EF, Hammell CM, Hodge CA, Cole CN (2005). Yeast poly(A)-binding protein, Pab1, and PAN, a poly(A) nuclease complex recruited by Pab1, connect mRNA biogenesis to export. Genes Dev 19, 90–103.

Ekwall, K. (2005). Genome-wide analysis of HDAC function. Trends Genet 21, 608–615.

Feuerbach F, Galy V, Trelles-Sticken E, Fromont-Racine M, Jacquier A, Gilson E, Olivo-Marin J-C, Scherthan H, Nehrbass U (2002). Nuclear architecture and spatial positioning help establish transcriptional states of telomeres in yeast. Nat Cell Biol 4, 214–221.

Fisk DG, Ball CA, Dolinski K, Engel SR, Hong EL, Issel-Tarver L, Schwartz K, Sethuraman A, Botstein D, Michael Cherry J, Project TGD (2006). Saccharomyces cerevisiae S288C genome annotation: a working hypothesis. Yeast 23, 857–865.

Galy V, Olivo-Marin JC, Scherthan H, Doye V, Rascalou N, Nehrbass U (2000). Nuclear pore complexes in the organization of silent telomeric chromatin. Nature 403, 108–112.

Glozak MA, Sengupta N, Zhang X, Seto E (2005). Acetylation and deacetylation of non-histone proteins. Gene 363, 15–23.

Green EM, Jiang Y, Joyner R, Weis K (2012). A negative feedback loop at the nuclear periphery regulates GAL gene expression. Mol Biol Cell 23, 1367–1375.

Grund SE, Fischer T, Cabal GG, Antúnez O, Pérez-Ortín JE, Hurt E (2008). The inner nuclear membrane protein Src1 associates with subtelomeric genes and alters their regulated gene expression. J Cell Biol 182, 897–910.

Grunstein M, Gasser SM (2013). Epigenetics in Saccharomyces cerevisiae. Cold Spring Harb Perspect Biol 5, a017491.

Harr JC, Gonzalez-Sandoval A, Gasser SM (2016). Histones and histone modifications in perinuclear chromatin anchoring: from yeast to man. EMBO Rep 17, 139–155.

Hodge CA, Choudhary V, Wolyniak MJ, Scarcelli JJ, Schneiter R, Cole CN (2010). Integral membrane proteins Brr6 and Apq12 link assembly of the nuclear pore complex to lipid homeostasis in the endoplasmic reticulum. J Cell Sci 123, 141–151.

Houseley J, Rubbi L, Grunstein M, Tollervey D, Vogelauer M (2008). A ncRNA modulates histone modification and mRNA induction in the yeast GAL gene cluster. Mol Cell 32, 685–695.

Huh W-K, Falvo JV, Gerke LC, Carroll AS, Howson RW, Weissman JS, O'Shea EK (2003). Global analysis of protein localization in budding yeast. Nat Cell Biol 425, 686–691.

Inada M, Nichols RJ, Parsa J-Y, Homer CM, Benn RA, Hoxie RS, Madhani HD, Shuman S, Schwer B, Pleiss JA (2016). Phospho-site mutants of the RNA Polymerase II C-terminal domain alter subtelomeric gene expression and chromatin modification state in fission yeast. Nucleic Acids Res 44, 9180–9189.

Janin A, Bauer D, Ratti F, Millat G, Méjat A (2017). Nuclear envelopathies: a complex LINC between nuclear envelope and pathology. Orphanet J Rare Dis 12, 147.

Kærn M, Elston TC, Blake WJ, Collins JJ (2005). Stochasticity in gene expression: from theories to phenotypes. Nat Rev Genet 6, 451–464.

Langmead B, Trapnell C, Pop M, Salzberg SL (2009). Ultrafast and memory-efficient alignment of short DNA sequences to the human genome. Genome Biol 10, R25.

Laporte D, Courtout F, Tollis S, Sagot I (2016). Quiescent Saccharomyces cerevisiae forms telomere hyperclusters at the nuclear membrane vicinity through a multifaceted mechanism involving Esc1, the Sir complex, and chromatin condensation. Mol Biol Cell 27, 1875–1884.

Lau AC, Zhu KP, Brouhard EA, Davis MB, Csankovszki G (2016). An H4K16 histone acetyltransferase mediates decondensation of the X chromosome in C. elegans males. Epigenetics Chromatin 9, 44.

Li H, Handsaker B, Wysoker A, Fennell T, Ruan J, Homer N, Marth G, Abecasis G, Durbin R, Subgroup GPDP (2009). The sequence alignment/map format and SAMtools. Bioinformatics 25, 2078–2079.

Liu Y, Lu C, Yang Y, Fan Y, Yang R, Liu C-F, Korolev N, Nordenskiöld L (2011). Influence of histone tails and H4 tail acetylations on nucleosome-nucleosome interactions. J Mol Biol 414, 749–764.
Lohr D, Venkov P, Zlatanova J (1995). Transcriptional regulation in the yeast GAL gene family: a complex genetic network. FASEB J 9, 777–787.
Lone MA, Atkinson AE, Hodge CA, Cottier S, Martínez-Montañés F, Maithel S, Mène-Saffrané L, Cole CN, Schneiter R (2015). Yeast integral membrane proteins Apq12, Brl1, and Brr6 form a complex important for regulation of membrane homeostasis and nuclear pore complex biogenesis. Eukaryot Cell 14, 1217–1227.
Love MI, Huber W, Anders S (2014). Moderated estimation of fold change and dispersion for RNA-seq data with DESeq2. Genome Biol 15, 550.
Luthra R, Kerr SC, Harreman MT, Apponi LH, Fasken MB, Ramineni S, Chaurasia S, Valentini SR, Corbett AH (2007). Actively transcribed GAL genes can be physically linked to the nuclear pore by the SAGA chromatin modifying complex. J Biol Chem 282, 3042–3049.
Martin, M. (2011). Cutadapt removes adapter sequences from high-throughput sequencing reads. EMBnet J 17, 10-12-13.
Mekhail K, Seebacher J, Gygi SP, Moazed D (2008). Role for perinuclear chromosome tethering in maintenance of genome stability. Nature 456, 667–670.
Millar CB, Kurdistani SK, Grunstein M (2004). Acetylation of yeast histone H4 lysine 16: a switch for protein interactions in heterochromatin and euchromatin. Cold Spring Harb Symp Quant Biol 69, 193–200.
Misteli T (2001). Protein dynamics: implications for nuclear architecture and gene expression. Science 291, 843–847.
Munchel SE, Shultzaberger RK, Takizawa N, Weis K (2011). Dynamic profiling of mRNA turnover reveals gene-specific and system-wide regulation of mRNA decay. Mol Biol Cell 22, 2787–2795.
Neems D, Kosak ST (2010). Turning down the volume on transcriptional noise. Nat Cell Biol 12, 929–931.
Oppikofer M, Kueng S, Martino F, Soeroes S, Hancock SM, Chin JW, Fischle W, Gasser SM (2011). A dual role of H4K16 acetylation in the establishment of yeast silent chromatin. EMBO J 30, 2610–2621.
Ptak C, Aitchison JD, Wozniak RW (2014). The multifunctional nuclear pore complex: a platform for controlling gene expression. Curr Opin Cell Biol 28, 46–53.
Quinlan AR (2014). BEDTools: the Swiss-army tool for genome feature analysis. Curr Protoc Bioinform 47, 11.12.11–34.
Raj A, Rifkin SA, Andersen E, van Oudenaarden A (2010). Variability in gene expression underlies incomplete penetrance. Nature 463, 913–918.
Rajapakse I, Groudine M (2011). On emerging nuclear order. J Cell Biol 192, 711–721.
Randise-Hinchliff C, Coukos R, Sood V, Sumner MC, Zdraljevic S, Meldi Sholl L, Garvey Brickner D, Ahmed S, Watchmaker L, Brickner JH (2016). Strategies to regulate transcription factor-mediated gene positioning and interchromosomal clustering at the nuclear periphery. J Cell Biol 212, 633–646.
Robinson PJJ, An W, Routh A, Martino F, Chapman L, Roeder RG, Rhodes D (2008). 30 nm chromatin fibre decompaction requires both H4-K16 acetylation and linker histone eviction. J Mol Biol 381, 816–825.
Rohner S, Gasser SM, Meister P (2008). Modules for cloning-free chromatin tagging in Saccharomyces cerevisae. Yeast 25, 235–239.
Rohner S, Kalck V, Wang X, Ikegami K, Lieb JD, Gasser SM, Meister P (2013). Promoter- and RNA polymerase II-dependent hsp-16 gene association with nuclear pores in Caenorhabditis elegans. J Cell Biol 200, 589–604.
Scarcelli JJ, Hodge CA, Cole CN (2007). The yeast integral membrane protein Apq12 potentially links membrane dynamics to assembly of nuclear pore complexes. J Cell Biol 178, 799–812.
Schmid M, Arib G, Laemmli C, Nishikawa J, Durussel T, Laemmli UK (2006). Nup-PI: the nucleopore-promoter interaction of genes in yeast. Mol Cell 21, 379–391.
Séron K, Blondel MO, Haguenauer-Tsapis R, Volland C (1999). Uracil-induced down-regulation of the yeast uracil permease. J Bacteriol 181, 1793–1800.
Shia W-J, Osada S, Florens L, Swanson SK, Washburn MP, Workman JL (2005). Characterization of the yeast trimeric-SAS acetyltransferase complex. J Biol Chem 280, 11987–11994.
Shogren-Knaak M, Ishii H, Sun J-M, Pazin MJ, Davie JR, Peterson CL (2006). Histone H4-K16 acetylation controls chromatin structure and protein interactions. Science 311, 844–847.
Sood V, Brickner JH (2014). Nuclear pore interactions with the genome. Curr Opin Genet Dev 25, 43–49.
Stancheva I, Schirmer EC (2014). Nuclear envelope: connecting structural genome organization to regulation of gene expression. Adv Exp Med Biol 773, 209–244.
Steglich B, Sazer S, Ekwall K (2013). Transcriptional regulation at the yeast nuclear envelope. Nucleus 4, 379–389.
Taddei A, Gasser SM (2012). Structure and function in the budding yeast nucleus. Genetics 192, 107–129.
Taddei A, Hediger F, Neumann FR, Bauer C, Gasser SM (2004). Separation of silencing from perinuclear anchoring functions in yeast Ku80, Sir4 and Esc1 proteins. EMBO J 23, 1301–1312.
Taddei A, Van Houwe G, Hediger F, Kalck V, Cubizolles F, Schober H, Gasser SM (2006). Nuclear pore association confers optimal expression levels for an inducible yeast gene. Nature 441, 774–778.
Tamm T, Grallert A, Grossman EPS, Alvarez-Tabares I, Stevens FE, Hagan IM (2011). Brr6 drives the Schizosaccharomyces pombe spindle pole body nuclear envelope insertion/extrusion cycle. J Cell Biol 195, 467–484.
Taylor GCA, Eskeland R, Hekimoglu-Balkan B, Pradeepa MM, Bickmore WA (2013). H4K16 acetylation marks active genes and enhancers of embryonic stem cells, but does not alter chromatin compaction. Genome Res 23, 2053–2065.
Torres EM, Sokolsky T, Tucker CM, Chan LY, Boselli M, Dunham MJ, Amon A (2007). Effects of aneuploidy on cellular physiology and cell division in haploid yeast. Science 317, 916–924.
Trapnell C, Pachter L, Salzberg SL (2009). TopHat: discovering splice junctions with RNA-Seq. Bioinformatics 25, 1105–1111.
Traven A, Jelicic B, Sopta M (2006). Yeast Gal4: a transcriptional paradigm revisited. EMBO Rep 7, 496–499.
Wei W, Pelechano V, Järvelin AI, Steinmetz LM (2011). Functional consequences of bidirectional promoters. Trends Genet 27, 267–276.
Wong X, Luperchio TR, Reddy KL (2014). NET gains and losses: the role of changing nuclear envelope proteomes in genome regulation. Curr Opin Cell Biol 28, 105–120.
Wu J, Suka N, Carlson M, Grunstein M (2001). TUP1 utilizes histone H3/H2B-specific HDA1 deacetylase to repress gene activity in yeast. Mol Cell 7, 117–126.
Zenklusen D, Singer RH (2010). Analyzing mRNA expression using single mRNA resolution fluorescent in situ hybridization. Methods Enzymol 470, 641–659.
Zhang R, Erler J, Langowski J (2017). Histone acetylation regulates chromatin accessibility: role of H4K16 in inter-nucleosome interaction. Biophys J 112, 450–459.
Zimmer C, Fabre E (2011). Principles of chromosomal organization: lessons from yeast. J Cell Biol 192, 723–733.